Self-ordering of random intercalates in thin films of cuprate superconductors: Growth model and x-ray diffraction diagnosis

D. Ariosa,[1] C. Cancellieri,[1] P. H. Lin,[1,2,3] and D. Pavuna[1]
[1]*Laboratory of X-ray, EPFL SB-IPMC-LPRX, CH-1015 Lausanne, Switzerland*
[2]*Department of Engineering and System Science, National Tsing Hua University, TW-30013, Taiwan*
[3]*Academia Sinica, Institute of Physics, TW-11529, Taiwan*
(Received 22 January 2007; published 3 May 2007)

We propose a simple model for the nucleation of random intercalates during the growth of high-temperature superconductor (HTSC) films by pulsed laser deposition (PLD). The model predicts a very particular spatial distribution of defects: a Markovian-like sequence of displacements along the growth direction (c axis), as well as a two-component in-plane correlation function, characteristic of self-organized intercalates. A model for x-ray diffraction (XRD) on such structures is also developed and accounts for both c-axis and in-plane anomalies observed in XRD experiments. The method presented in this work constitutes a useful characterization tool in the optimization of deposition parameters for the growth of HTSC films.

DOI: 10.1103/PhysRevB.75.184505 PACS number(s): 61.10.Nz, 68.55.Ln, 81.15.Aa, 81.15.Fg

I. INTRODUCTION

The observation of random intercalates is recurrent in both natural and artificial layered materials. The class of materials subject to random intercalation is very large: it ranges from graphite[1] and interstratified clay minerals[2,3] to high-temperature superconductors (HTSC).[4–7] Although the present work may apply to a large variety of materials, we will focus our discussion on HTSC and, more specifically, on $Bi_2Sr_2CuO_6$ (Bi-2201) thin films grown by pulsed laser deposition (PLD). Indeed, compounds of the $Bi_2Sr_2Ca_nCu_{n+1}O_{2n+6}$ (BSCCO) family, as most HTSC, are cuprates with a characteristic layered perovskite structure. The BSCCO family constitutes a good example of intergrowth formation. Namely, these materials tend to form polytypes,[8] since the formation enthalpy of a compound, e.g., the Bi-2201 with a single CuO_2 layer, differs only slightly from that of the two CuO_2 layer-compound Bi-2212. In addition, growth of films by PLD is an out-of-equilibrium process,[9,10] which favors the irreversible formation of otherwise metastable intercalates.

In Sec. II we present a phenomenological model for irreversible random nucleation of intergrowth (guest phase) during the layer formation of a given compound (host phase). The structure and composition of the guest phase are assumed to be very similar to the structure and composition of the host phase; the main difference being their respective lattice constant in the growth direction (z axis). The energy cost of such random intercalation has two contributions: a chemical contribution (formation enthalpy difference), as well as an elastic contribution which penalizes the relative z-axis displacement of in-plane adjacent unit cells (steps). The associated dynamics is studied by combining a mean-field approach and a numerical simulation. The result is a Markovian sequence of layers containing, following a short transient, a constant amount of guest unit cells and steps per layer. In Sec. III we derive the corresponding c-axis and in-plane distributions and correlation functions, which we use in Sec. IV, to calculate and discuss x-ray diffraction (XRD) patterns by extending the method used in a previous publication on intercalated YBaCuO films.[7] The type of disorder generated by our simple model accounts for two characteristic XRD anomalies observed in various HTSC films: nonmonotonous deviations of Bragg peak positions (as well as peak broadening) and the appearance of two distinct contributions to the rocking curves (RCs), reflecting the self-ordering of in-plane defects. A concrete example is given for an intercalated Bi-2201 thin film. Finally, we summarize the main points and draw the conclusions in Sec. V.

II. MODEL

The following phenomenological model describes the intergrowth of metastable intercalates during the deposition of a layered material from its vapor phase. The basic assumptions of the model are as follows:

(i) The global stoichiometry of the vapor phase is the one of the desired host phases.

(ii) The random nucleation of guest unit cells (GUCs) is induced by local composition fluctuations in the top layer under formation enthalpy and is favored by the reduced in-plane mobility of certain species and the small difference between the formation enthalpies.

(iii) The GUC nucleation depends on two parameters: the formation enthalpy difference $V=E_G-E_H$ and the energy per step U. We assume that the in-plane footprint of the guest and the host is the same, allowing for a perfect epitaxial growth along the c axis. The step (see Fig. 1), defined as a lateral mismatch induced by a finite relative displacement between in-plane adjacent UC, implies a local strain field with its corresponding elastic energy cost.

(iv) The GUC nucleation rate on a given site obeys local thermodynamic equilibrium.

The basic assumptions of our model are minimal, in the sense that we aim to investigate only two basic features of the intergrowth formation: the displacement distribution $P_t(z)$ of the UCs along the c axis and the average in-plane two-point correlation function of the displacements $g(x)=\langle g_t(x)\rangle$, where $g_t(x)$ is the correlation function on a given

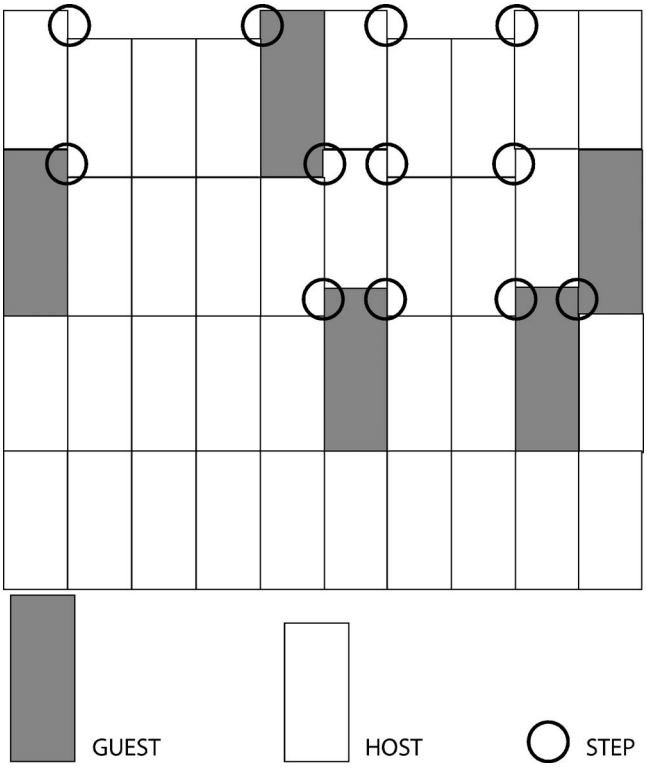

FIG. 1. Schematic film cross section; formation of steps by random nucleation of GUC.

layer indexed by t. The minimal approach is justified by the fact that only the Fourier transforms of these two quantities have a direct impact on the standard XRD patterns of thin films. In order to investigate the displacement distribution along the growth direction (z axis), we use a mean-field (MF) approach. Although the layer-by-layer growth is a two-dimensional (2D) process, within the MF approach we can map the system on an effective one-dimensional (1D) system (row by row) by integrating over one in-plane degree of freedom. While the MF approach is well adapted for a description of the z-axis sequencing and correlations, it masks all information about the in-plane spatial correlations. In order to investigate the in-plane disorder, we implement a numerical simulation of the complete 2D model.

A. Mean-field approach

In order to derive a mean-field-like rate equation for the steps, we have to examine different events that may occur during the construction of a given layer, and their corresponding Boltzmann probabilities. The nucleation of a GUC on top of the former layer depends on the neighboring environment of the considered site, as schematically depicted in Fig. 2. Starting with a 2D model (the upper part of Fig. 2) and provided the next-neighboring sites are filled with the majority phase–host unit cells (HUCs)—if the site belongs to a plateau (type a), the nucleation of a GUC will incorporate four additional steps to the system. The corresponding energy cost is $\Delta E = V + 4U$. For a site of type b, only two additional steps are incorporated; thus, the energy cost is ΔE

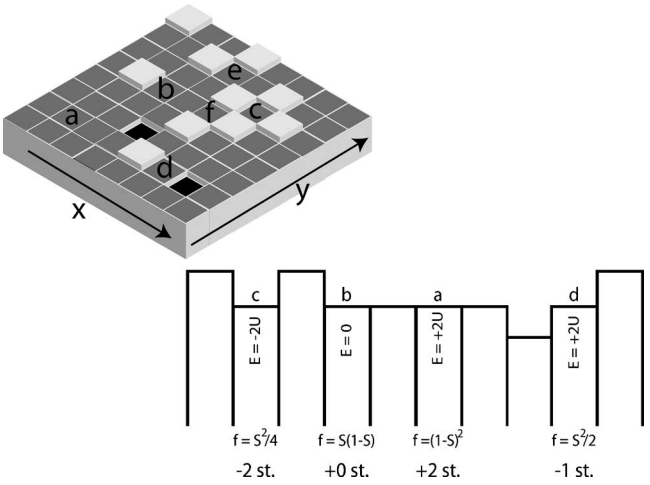

FIG. 2. Different site environments in 2D and their 1D restriction with the corresponding fractions f, energy costs E, and step number variations.

$= V + 2U$, etc. To reduce the 2D layer model to 1D, we have to average over all the possible configurations along the transversal direction (say y). As a result, configurations such as b, e, and f in the 2D layer are averaged to obtain the b configuration in the 1D row (lower part of Fig. 2) with an extra formation energy, corresponding to the weighted average of the elastic energy contributions from the corresponding transversal configurations. Assigning to them zero probability, we exclude from the analysis all the events that imply energy costs larger than $4U$. This assumption is justified by the fact that the high-energy costs of such events make their contribution statistically negligible. The fraction of each of the four types of sites, retained for the intergrowth nucleation, can be written in terms of the total 1D density of steps S within the given row,

$$f_{plateau} = (1 - S)^2, \tag{1}$$

$$f_{step} = (1 - S)S, \tag{2}$$

$$f_{valley} = \frac{1}{4}S^2, \tag{3}$$

$$f_{stair} = \frac{1}{2}S^2. \tag{4}$$

Equation (1) is the probability of finding two consecutive step-free sites. The total density of single steps being $2(1 - S)S$ in Eq. (2), we have excluded two types of sites (upper terraces) among the four possible situations close to a single step. The factors $\frac{1}{4}$ in Eq. (3) and $\frac{1}{2}$ in Eq. (4) account for the exclusion of one undesired type of site among the four possible double-step sites (probability S^2), retaining only the valley and staircase configurations. Within the 1D reduced system, the formation enthalpy difference V is renormalized as follows:

$$\tilde{V} = V + 2U\left[(1-S)^2 + \frac{1}{4}S^2\right]. \quad (5)$$

The rate equation can now be constructed for the effective row-by-row growth: If the site belongs to a plateau (a), the nucleation of a GUC will incorporate two additional steps to the system. Conversely, if the site is already on the low displacement terrace of a single step (b), there will be no additional steps but just a shift of the existing one. If the site belongs to a valley (c), i.e., to low displacement terrace between two consecutive steps, the GUC nucleation will remove two steps from the system. Finally, if the site belongs to a staircase configuration (d), the GUC nucleation will remove one step, but the remaining steps will be double sized (elastic energy=$4U$).

The local equilibrium condition (iv) is implemented by using the Boltzmann factors u and $\tilde{v}$ corresponding to the energies U and $\tilde{V}$, respectively,

$$u = \exp(-U/k_BT), \quad \tilde{v} = \exp(-\tilde{V}/k_BT). \quad (6)$$

Therefore, with the correct normalization, the thermal probabilities for intergrowth nucleation at different sites are

$$p_0 = \frac{\tilde{v}u^2}{1+\tilde{v}u^2}, \quad p_1 = \frac{\tilde{v}}{1+\tilde{v}}, \quad p_2 = \frac{\tilde{v}}{\tilde{v}+u^2}, \quad p_3 = p_0, \quad (7)$$

where subindices 0, 1, 2, and 3 stand for plateau, single step, valley, and staircase, respectively. Only events 0, 2, and 3 induce variations on S, while event 1 does not alter the number of steps. The balance in a given row yields the sought rate equation,

$$\frac{dS}{dt} = 2\left[p_0(1-S)^2 - \frac{1}{4}(p_2+p_3)S^2\right]. \quad (8)$$

In Eq. (8), the "time" variable t has to be interpreted as an integer layer index. The expression for the general solution of the above differential equation reads as follows:

$$S = S_0 + S_1 \tanh[\nu(t-t_0)]. \quad (9)$$

By differentiating Eq. (9), the parameters S_0, S_1, and ν can be found by comparison with Eq. (8),

$$S_0 = \frac{4u^2}{3u^2 - \dfrac{1+\tilde{v}u^2}{\tilde{v}+u^2}}, \quad S_1 = \pm\frac{2u\sqrt{u^2+\dfrac{1+\tilde{v}u^2}{\tilde{v}+u^2}}}{3u^2-\dfrac{1+\tilde{v}u^2}{\tilde{v}+u^2}},$$

$$\nu = \mp\frac{\tilde{v}u\sqrt{u^2+\dfrac{1+\tilde{v}u^2}{\tilde{v}+u^2}}}{1+\tilde{v}u^2}. \quad (10)$$

The first layer grows on a step-free substrate. The parameter t_0 is then defined by this initial condition,

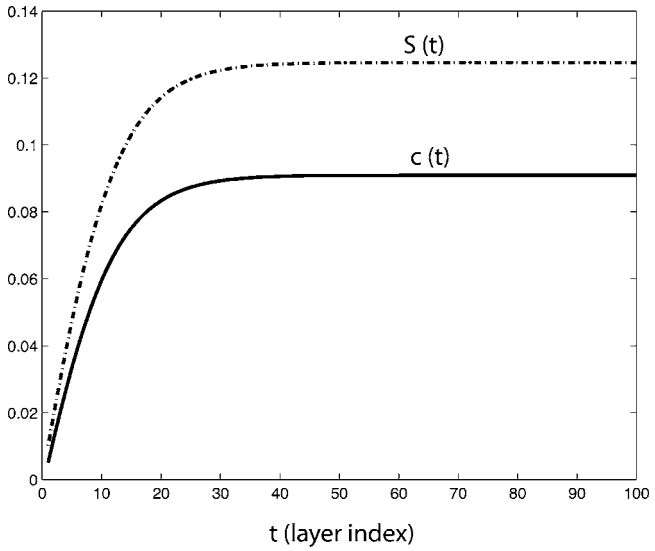

FIG. 3. Evolution of layer step density S and GUC density c with film thickness t.

$$S(1) = 2p_0 \Rightarrow t_0 = 1 - \frac{1}{\nu}\tanh^{-1}\left(\frac{2p_0 - S_0}{S_1}\right). \quad (11)$$

The concentration c of GUC within a given layer depends on the distribution of steps in the preceding layer,

$$c(t+1) = p_0(1-S)^2 + \frac{1}{4}(p_2+2p_3)S^2 + p_1S(1-S). \quad (12)$$

The existence of a steady-state regime follows directly from Eq. (8),

$$\frac{dS}{dt} = 0 \Leftrightarrow S = \frac{2u\sqrt{\dfrac{\tilde{v}+u^2}{1+2u^2\tilde{v}+u^4}}}{1+2u\sqrt{\dfrac{\tilde{v}+u^2}{1+2u^2\tilde{v}+u^4}}} \equiv \bar{S}. \quad (13)$$

Accordingly, by inserting $\bar{S}$ into Eq. (12), we obtain the asymptotical GUC concentration,

$$\bar{c} = 2p_0(1-\bar{S})^2 + p_1\bar{S}(1-\bar{S}) + \frac{1}{4}p_0\bar{S}^2. \quad (14)$$

The extension of the transient is governed by the parameter ν through a characteristic length (number of layers) $\tau=\frac{1}{\nu}$. The lowest value τ can attain (rapid approach to the steady state) is $\tau_{min}=\left|\frac{1+v}{\sqrt{2}v}\right|$, and it corresponds to the extreme situation where the (elastic) energy per step is $U=0$. In this limit, the dynamics is only determined by the difference in the formation enthalpy V. In the other extreme, when $U \gg |V|$ (large step energy), in the initial stage of the growth $\tilde{V} \simeq 2U$ and τ scales with $1/u^2 \gg 1$. In any case, for intermediate situations (say, $\frac{U}{k_BT} \approx \frac{|V|}{k_BT} \simeq 1$), τ will be of the order of a few tens of layers. The latter is illustrated in Fig. 3, where we plotted $S(t)$ and $c(t)$ according to Eqs. (9)–(12), using parameter values taken from a fit of an actual Bi-2201 thin film sample:[11] $\frac{V}{k_BT}=-6.17$ and $\frac{U}{k_BT}=+3.22$. These values imply, at

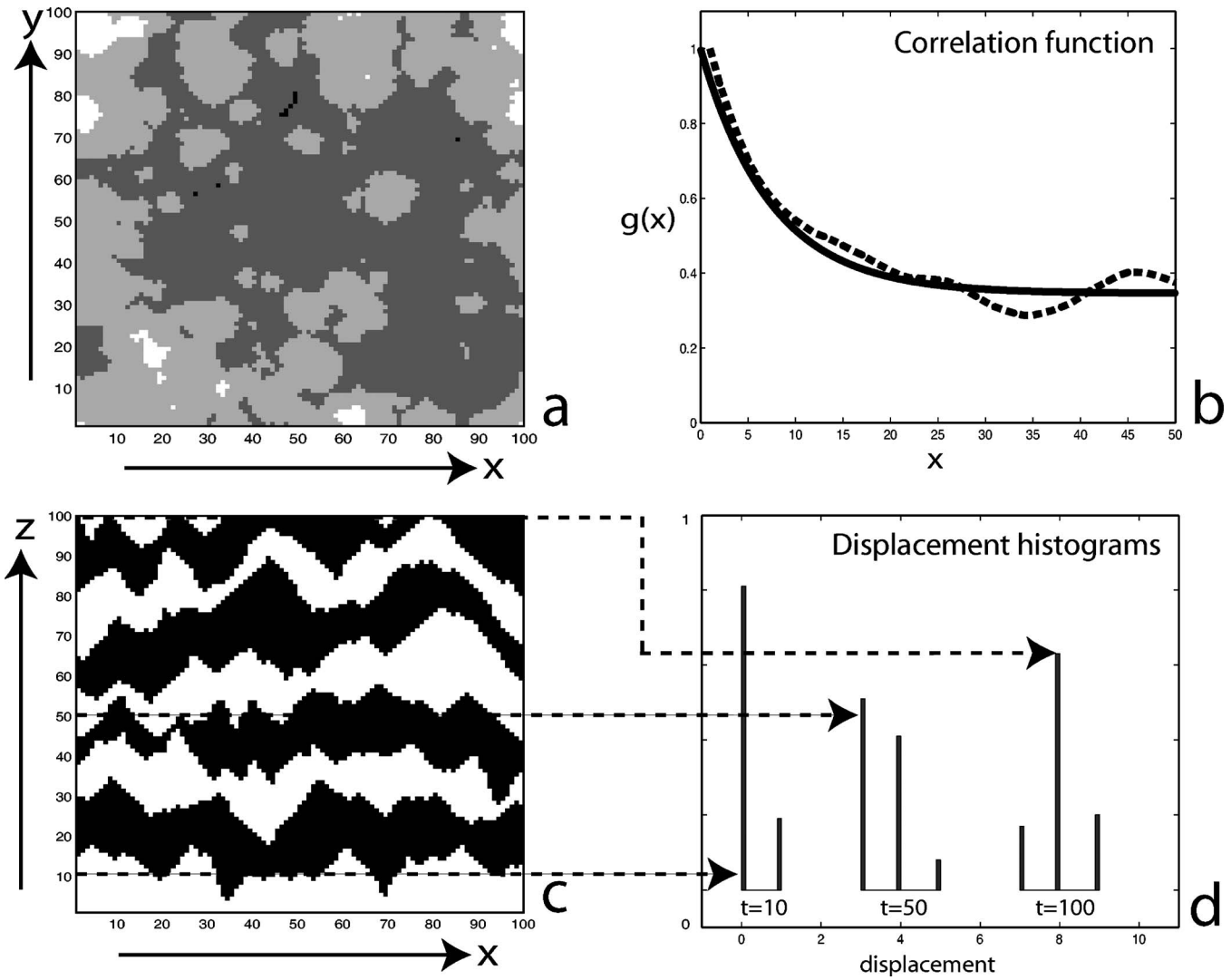

FIG. 4. Numerical simulation: (a) top view of the last layer, (b) in-plane correlation function and its fit (solid line) using Eq. (22), (c) film cross section (x-z plane), and (d) displacement histograms for layers 10, 50, and 100.

a substrate temperature of 640 °C, $V=-0.49$ eV and $U=+0.25$ eV. In terms of standard enthalpy differences, this value of $|V|$ for a single GUC corresponds to 47 kJ/mol and is in the same order of magnitude as the 20 kJ/mol difference between Bi-2212 and Bi-2223.[12] Concerning the value of U, by using the lattice constants of Bi-2201,[13] we find a stacking fault energy of 85 mJ/m^2, again realistic order of magnitude for oxides ($\sim$100 mJ/m^2).

B. Numerical simulation

We have run the standard Metropolis algorithm commonly used in Monte Carlo (MC) simulations using the Boltzmann rates as defined in Eq. (6), for the same model parameters as in Fig. 3. However, the difference with a real MC simulation is that, after an event (HUC or GUC) is chosen on a given site, there is no further update at the site. Under such conditions, the simulation reproduces the irreversibility of the phenomenon, and the result does not represent a global thermodynamic equilibrium.

Figure 4 shows the numerical simulation of a 100-layer film grown according to the model described above. Each layer consists of a 100×100 array with periodic boundary conditions. Figure 4(a) is a map of equally displaced domains on a given layer (top view). Figure 4(b) is the in-plane two-point correlation function averaged over the top layer. Figure 4(c) is a vertical cross section of the film, in which different displacement domains are successively colored in black and white. Histograms in Fig. 4(d) are computed at three different stages of film formation. One can already notice from Figure 4(a) the in-plane clustering of equally displaced domains. More detailed discussion of the simulation results is given in the next section in connection with the evaluation of the correlation functions.

III. DISPLACEMENT DISTRIBUTIONS AND CORRELATION FUNCTIONS

A. Displacement distribution along z

In the steady state, the distribution along z can be cast in terms of the density c of GUC. Let us denote the host and the

guest c-axis parameters as c_0 and c_1, respectively. The probability density distribution for the position along z of a UC in the layer t obeys the following recursion relation:[7,14]

$$P_t(z) = (1-c)P_{t-1}(z-c_0) + cP_{t-1}(z-c_1). \tag{15}$$

Equation (15) simply means that a UC within the layer t will end at z with probability $(1-c)$ (hence, with lattice constant c_0) provided the underlying UC has ended at $z-c_0$ or with probability c (with lattice constant c_1) provided the underlying UC has ended at $z-c_1$. The initial condition (growing on an empty substrate) can be written as follows:

$$P_1(z) = (1-c)\delta(z-c_0) + c\delta(z-c_1). \tag{16}$$

The distribution finally reads

$$P_t(z) = \sum_{n=0}^{t} \binom{t}{n} c^n (1-c)^{t-n} \delta(z - tc_0 - n\Delta), \tag{17}$$

where $\Delta \equiv c_1 - c_0$ is the difference between the two lattice constants and $\binom{t}{n}$ are the binomial coefficients. Notice that, even in the steady state, the standard deviation of such a distribution is monotonically increasing with the layer index t. The latter is illustrated by the histograms in Fig. 4(d) which have been computed at three different stages of the film formation: t= 10, 50, and 100. They are a particular stochastic realization of Eq. (17).

For later use within the XRD context, it is also useful to compute the Fourier transform $P_t(q)$ of $P_t(z)$. The Fourier transform of the recursion relation [Eq. (15)] immediately gives

$$P_t(q) = [P_1(q)]^t = \{[(1-c) + ce^{-iq\Delta}]e^{-iqc_0}\}^t. \tag{18}$$

B. In-plane correlations

In Fig. 4(a) we have mapped equally displaced domains for the top layer (t=100) of our simulated film: each gray level corresponds to a given displacement value. Figure 4(c) is a vertical cross section of the film in which we have assigned the white or black color to cells with an even or odd number of displacements, respectively. Consequently, it is easier to visualize the horizontal borders between two adjacent domains. These borders contain *a fortiori* a GUC and show a staircase structure. One can describe Fig. 4(a) as a domain with displacement value of 8Δ, containing inclusions with displacement values of 7Δ and 9Δ. The clustered structure in Fig. 4(a) is in striking contrast with the homogeneous mixture of displacement values one would expect from a completely random intergrowth nucleation in the U=0 limit. Indeed, for a given value of the GUC concentration, both the clustered structure of the domains and the staircase arrangement of GUC reduce the number of steps and the associated elastic energy. The corresponding in-plane two-point correlation function $g(x)$, plotted in Fig. 4(b), shows a rapid exponential drop over the first 20 sites, followed by a constant asymptotic behavior for larger distances. The exponential contribution to $g(x)$ is similar to the usual short-range correlation due to stacking faults in epitaxial films. The constant contribution is less usual and denotes a spatially independent (infinite range) correlation. Focusing on a single layer, one has then to consider correlations on two distinct length scales: short-range correlations for cells belonging to the same cluster, and space-independent correlations for cells situated on different clusters anywhere within the same layer. Let us denote the short-range correlation function as $g_1(x)$: it is the probability for two cells, within a given layer and at a distance $|x|$ of each other, to belong to the same displacement domain, i.e., with no steps in between. The general form for $g_1(x)$ reads as follows:

$$g_1(x) = e^{-|x|/\xi}, \tag{19}$$

Equation (19) contains a characteristic decay distance ξ, corresponding to the average domain linear size. This characteristic distance depends not only on the step concentration S but also on the in-plane step distribution characterizing the cluster's structure. While the value of ξ cannot be computed within the MF approach, a lower bound can be found, corresponding to the homogeneous step distribution situation (U =0),

$$g_1(x) = (1-S)^{|x|/a} = e^{-|x|/\xi} \Rightarrow \xi_{min} = \frac{a}{\ln\left(\frac{1}{1-S}\right)}, \tag{20}$$

where a is the in-plane lattice constant. In the case of the real sample used as an example in the present contribution, the steady-state value for the step concentration is S=0.12 (see Fig. 3), implying $\xi_{min} \approx 8UC$, approximately half the value observed in the numerical simulation.

The evaluation of the space-independent correlation g_0 follows directly from the MF z-axis distribution [Eq. (17)],

$$g_0 = \frac{1}{N}\sum_{t=1}^{N} \int_{tc_0}^{tc_1} [P_t(z)]^2 dz = \frac{1}{N}\sum_{t=1}^{N}\sum_{n=0}^{t} \left[\binom{t}{n} c^n (1-c)^{t-n} \right]^2. \tag{21}$$

In Eq. (21), $[P_t(z)]^2$ is the probability of finding two cells, within the layer t, having the same z-axis position (i.e., containing the same number of intergrowth in their underlying columns) regardless of their particular mutual in-plane distance. The integration over $z \in [tc_0, tc_1]$ gives the total probability of finding two such cells for any possible displacement within the t layer. g_0 is then obtained by averaging over the entire film (N layers) of the preceding quantity. The evolution of g_0 with the total number of layers is depicted in Fig. 5 for the same model parameters as before, calculated according to Eq. (21). Notice that the space-independent correlation is continuously decreasing with film thickness even in the steady state and that, as for the cluster's linear size ξ, Eq. (21) underestimates g_0. The latter is due to the fact that expression (17) is a MF result that does not take into account in-plane correlations; it describes just the random sequencing along the z axis.

Finally, the total two-point in-plane correlation function for displacements is given by

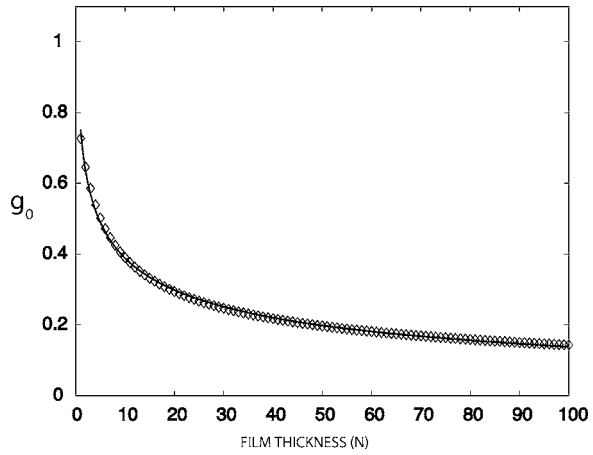

FIG. 5. Average space-independent correlation function vs film thickness from Eq. (21).

$$g(x) = g_1(x) + [1 - g_1(x)]g_0 = g_0 + (1 - g_0)g_1(x) = g_0 + (1 - g_0)e^{-|x|/\xi}. \quad (22)$$

The continuous line curve in Fig. 4(d) is a fit obtained by using expression (22).

IV. X-RAY DIFFRACTION

For epitaxial thin film characterization with an x-ray diffractometer, the most common measurements are θ-2θ scans (T2T) and RC.[15] The first technique, also known as the Bragg-Brentano geometry, consists of measurements of the diffracted intensity by keeping the sample's surface normal at the bisecting position between the incident and diffracted beams. In the second one, the detector is fixed in a Bragg position $2\theta_B$, and the sample surface is slightly rotated around the bisecting position $\Omega = \theta_B$. Therefore, T2T scans probe the crystal along the normal direction, while RCs do it along the sample's in-plane direction, contained in the plane of the two beams.

A. θ-2θ scans

1. Deviation of Bragg peak positions

The relation between q, the modulus of the momentum transfer vector, and the diffraction angle 2θ in Bragg-Brentano geometry is

$$q = \frac{4\pi \sin(\theta)}{\lambda}, \quad (23)$$

where λ is the wavelength of the monochromatic x-ray beam. The diffraction amplitude from a c-axis-oriented perfect periodic crystal reads

$$A(q) = f_{UC}(q)\sum_{t=1}^{N} e^{-iqtc_0} \to f_{UC}(q)\sum_n \delta\left(q - n\frac{2\pi}{c_0}\right), \quad N \to \infty, \quad (24)$$

where $f_{UC}(q)$ is the structure factor of the crystal UC and N the total number of UCs along the c axis. The intensity diffracted by a perfect crystal, which is proportional to the square modulus of the amplitude [Eq. (24)], presents equally spaced Bragg peaks at each $q = nq_0$, with $q_0 = 2\pi/c_0$. The sum over the periodic layered structure appearing in the first equality of Eq. (4) is strongly modified if the beam encounters randomly displaced UCs in the intercalated crystal, as discussed elsewhere.[7] In order to compute the diffracted amplitude for a crystal containing random intergrowth, we have to perform its average over the displacement distribution $P_t(z)$,

$$\langle A(q)\rangle = \overline{f_{UC}(q)}\sum_{t=1}^{N}\langle e^{-iqz(t)}\rangle = \overline{f_{UC}(q)}\sum_{t=1}^{N}\int P_t(z)e^{-iqz}dz = \overline{f_{UC}(q)}\sum_{t=1}^{N} P_t(q). \quad (25)$$

In Eq. (25), the average of the phase factor and the UC structure factor have been computed independently since the displacement and the nature of the UC are independent random events. The mean structure factor is simply the weighted average of guest and host structure factors,

$$\overline{f_{UC}(q)} = (1 - c)f_{HUC}(q) + cf_{GUC}(q). \quad (26)$$

Inserting Eq. (18) in Eq. (25), the expression for the diffraction amplitude reads

$$\langle A(q)\rangle = \overline{f_{UC}(q)}\sum_{t=1}^{N}[(1 - c) + ce^{-iq\Delta}]^t e^{-iqtc_0}. \quad (27)$$

Comparing the above result with the first equality in Eq. (24), the main difference is the complex coefficient affecting the phase factor e^{-iqtc_0} in Eq. (27). This coefficient brings a phase correction for each term in the sum and its exponentially decaying amplitude enhances the weight of low index terms. As a result, the maxima in the diffracted intensity are shifted from their regular positions, and the angular-dependent anomalous peak broadening and intensity attenuation are observed in random intercalated films. The evaluation of the order-dependent deviations for peak positions requires rewriting of the additional complex coefficient in Eq. (27) in terms of modulus and phase,

$$(1 - c) + ce^{-iq\Delta} = R(q)e^{-i\varphi(q)}, \quad (28)$$

$$\text{with} \quad R(q) = \sqrt{1 - 2c(1 - c)[1 - \cos(q\Delta)]} \quad (29)$$

$$\text{and} \quad \varphi(q) = \arctan\left[\frac{\sin(q\Delta)}{\frac{1 - c}{c} + \cos(q\Delta)}\right]. \quad (30)$$

Consequently,

$$\langle A(q)\rangle = \overline{f_{UC}(q)}\sum_{t=1}^{N} R(q)^t \exp[-i\phi(q)t], \quad (31)$$

where $\phi(q)$ is the modified phase defined as

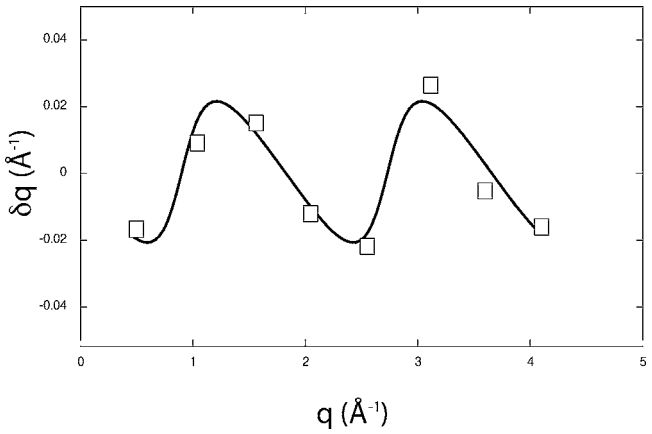

FIG. 6. Fitting the peak position deviations with Eq. (33).

$$\phi(q) = qc_0 + \varphi(q). \tag{32}$$

Since the real coefficient $R(q)$ is a slowly varying function in the vicinity of a peak, the maxima occur when all the terms of the sum in Eq. (31) contribute in phase, i.e., when $\phi(q_n) = 2n\pi$. The deviation δq of the Bragg peak position at any order can be calculated as follows:

$$\delta q \equiv q_n - nq_0 = q_n - n\frac{2\pi}{c_0} = -\frac{1}{c_0}\arctan\left[\frac{\sin(q\Delta)}{\frac{1-c}{c} + \cos(q\Delta)}\right]. \tag{33}$$

Measuring the subtle peak position deviations from an apparently single-phase-oriented film reveals the existence of the intergrowth. By fitting such deviations with Eq. (33), one can extract the total concentration c of the guest phase and the c-axis difference Δ with respect to the host material. An example is shown in Fig. 6 for a thin La-doped Bi-2201 film grown by laser ablation under conditions that enhance the intergrowth formation.[11] From the fit in Fig. 6, we obtained the following values: $c=0.18$ and $\Delta=3.7$ Å. This result has to be interpreted by considering the Bi-2201 symmetry (space group $I4/mmm$). Indeed, for the layer formation process, what matters is the building block with the reduced c axis ($c_0/2$), corresponding to one-half of the crystallographic UC we have used to index the diffraction peaks. In other words, 18% of intercalates corresponds to an actual amount of ≈9% of GUCs. The value of Δ is remarkably close to the typical lattice constant of cubic perovskites.

2. Anomalous peak broadening and weakening of intensity

Unlike in the case of perfect crystals, the sum in Eq. (31) does not cancel out away from the peak maximum. This is the reason why peak broadening is enhanced in a nonmonotonous way and also for the anomalous intensity modulation in random intercalated materials. These effects are controlled by the real coefficient $R(q)^t$ and its dependence on the summation index t. Performing the geometrical sum in Eq. (31) and calculating the corresponding intensity, one obtains

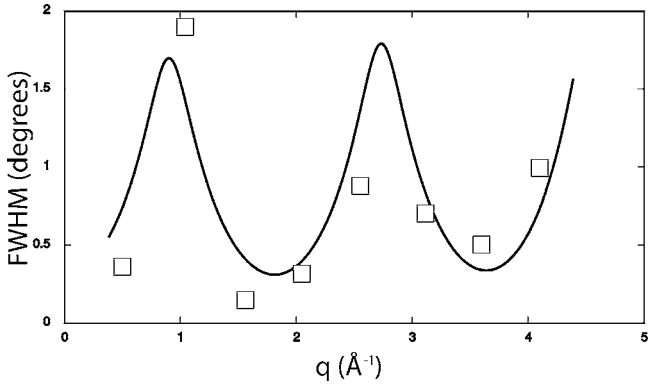

FIG. 7. Fitting the FWHM with Eq. (36).

$$I(q) = |\langle A(q)\rangle|^2 = \frac{|\overline{f_{UC}(q)}|^2}{1 + R^2(q) - 2R(q)\cos\phi(q)}, \tag{34}$$

where the extra q-dependent intensity modulation appears explicitly in the denominator. From Eq. (34), we can extract the full width at half maximum (FWHM) of the modified Bragg peaks. Indeed, the FWHM in Bragg-Brentano geometry is defined as $4\partial\theta$, where $\partial\theta$ is the deviation from θ_B resulting in a reduction of the scattered intensity by a factor of 2. The corresponding deviation $\partial\phi$ of the total phase obeys

$$2R[1-\cos(\partial\phi)] = (1-R)^2 \Rightarrow \partial\phi = \frac{4\pi c_0 \cos\theta}{\lambda}\partial\theta = \arccos\left[1 - \frac{(1-R)^2}{2R}\right]. \tag{35}$$

Finally, $\Delta(2\theta)$ (the FWHM) can be written as

$$\Delta(2\theta) = 4\partial\theta = \frac{\lambda}{\cos\theta}\left\{\frac{1}{t_{eff}} + \frac{1}{\pi c_0}\arccos\left[1 - \frac{(1-R)^2}{2R}\right]\right\}, \tag{36}$$

where the instrumental broadening has been neglected and the term $\frac{1}{t_{eff}}$ has been added to account for the effective size effect (Scherrer's formula).[15] In Fig. 7 we use the same fitting parameters c and Δ, as in Fig. 6. For the effective thickness, we find $t_{eff} \approx 300$ Å. This value, ten times smaller than the actual total thickness of the film (≈4000 Å), is the characteristic length over which the phase coherence is destroyed by disorder. This happens over distances for which the accumulated average displacement corresponds to one reduced UC ($c_0/2$). For the values found for c and Δ, one expects an effective coherence length $t_{eff} = \frac{c_0^2}{2c\Delta} = 447$ Å, in good agreement with the value used for the fit in Fig. 7.

B. Anomalous rocking curves

The signature, in XRD, of the very peculiar in-plane two-point correlation function discussed in Sec. III B would be the observation of two distinct contributions to the RC. It is well known that RC probes the in-plane crystal coherence and can have different shapes depending on the type of dis-

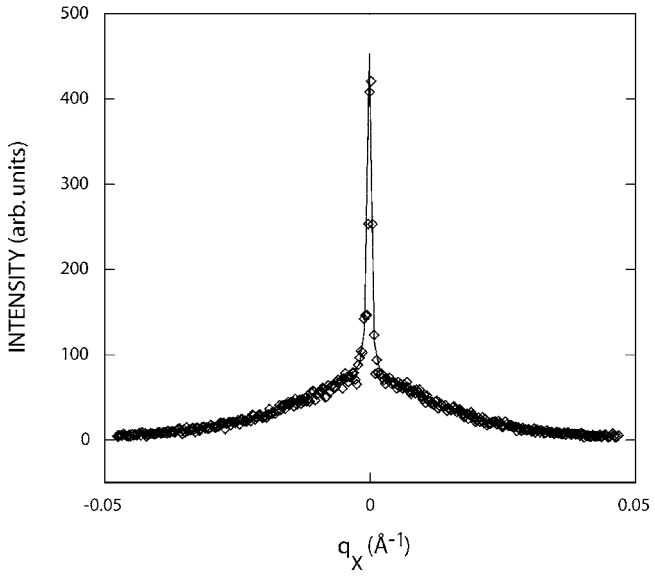

FIG. 8. Fitting the RC with Eq. (37).

order involved.[16] The RC is proportional to the Fourier transform of the two-point correlation function thus, from Eq. (22), we expect the RC to be a superposition of a Lorentzian curve generated by the exponential term and a Dirac peak generated by the constant term. The latter is, in fact, a narrow Lorentzian limited by the instrumental resolution.

The Fourier transform of Eq. (22) yields

$$g(q_x) = g_0\delta(q_x) + 2\xi(1-g_0)\frac{1}{1+(\xi q_x)^2}. \tag{37}$$

The FWHM of the Lorentzian Δq_x is given by

$$\Delta q_x = \frac{2}{\xi}. \tag{38}$$

Figure 8 is the fit of the RC on the (006) peak of the same film as above using Eq. (37). The value found for the fitting parameter is $\Delta q_x = 0.03$ Å^{-1}. According to Eq. (38), the in-plane coherence length seen by XRD is then $\xi = 67$ Å, corresponding to 17 UCs, in good agreement with the result of the numerical simulation. The integrated intensity ratio of the two contributions can be computed from Eq. (37),

$$r = \frac{\int g_0\delta(q_x)dq_x}{\int \frac{2\xi(1-g_0)}{1+(\xi q_x)^2}dq_x} = \frac{g_0}{2\pi(1-g_0)}. \tag{39}$$

Measuring the integrated intensity ratio on the RC ($r = 0.12$), we can extract the value of the space-independent correlation: $g_0 = 0.43$, again in good agreement with the numerical simulation [see Fig. 4(b)], showing the consistency of the approach.

V. CONCLUSIONS

Within the context of epitaxial growth of HTSC-layered oxides, we have developed a simple model for the random nucleation of intergrowth during the deposition of thin films by PLD. The model describes an out-of-equilibrium process, governed by two characteristic energies: the formation enthalpy difference and a "stacking fault" energy of elastic origin. A mean-field treatment allows us to find the displacement distribution along the growth direction and to show the existence of a steady state with a constant amount of intergrowth per layer. A numerical simulation, based on MC techniques, has been implemented in order to describe the in-plane disorder. We show that the z-axis displacements in the successive layers are self-organized in huge interpenetrating clusters. This result is directly interpreted within our model by noticing that this kind of structure reduces the elastic energy due to stacking faults, as compared with the homogeneous dilution of different displacement values. Consequently, the intergrowth is also self-organized in a staircase structure. The resulting in-plane two-point correlation function for the displacements consists of two components corresponding to two distinct length scales.

XRD patterns obtained from the calculated structure predict, for the T2T diffractograms, periodic deviations of the Bragg peaks from their regular positions, anomalous intensity modulations, and oscillating peak broadening. The RC shows two distinct contributions generated by the two components of the in-plane correlation function. Fitting XRD patterns with the above model allows us to measure the concentration c of intergrowth, the difference in lattice constants with respect to the host (z-axis displacement unit Δ), and the average in-plane cluster size.

The structural characterization of thin films is an unavoidable step in order to interpret their physical properties. Epitaxial intergrowth of isostructural parent compounds is a typical hidden defect that does not appear when using standard techniques. Observing closely, even single crystals, one realizes that the random intergrowth is often present. In the particular context of angle-resolved photoemission spectroscopy, the latter can bias the results as well as the interpretation of the electronic structure. In this context, our contribution provides a useful tool to control the quality and characterize the disorder in layered oxides.

ACKNOWLEDGMENTS

This work was supported by the Swiss National Science Foundation, the EPFL, and the National Science Council of Republic of China under Grant No. NCS 2917I007002.

[1] M. J. Winokur and R. Clarke, Phys. Rev. Lett. **56**, 2072 (1986).
[2] D. M. C. MacEwan, Nature (London) **171**, 616 (1953).
[3] D. M. C. MacEwan, Kolloid-Z. **149**, 96 (1956).
[4] Yu. M. Bakov, Phys. Solid State **42**, 1026 (2000).
[5] R. Borner, W. Paulus, R. Schollhorn, B. Kabius, and J. Schubert, Adv. Mater. (Weinheim, Ger.) **7**, 55 (1995).
[6] W. Paulus, R. Borner, R. Schollhorn, J. Schubert, W. Zander, J. Erxmaier, and A. Weidinger, Adv. Mater. (Weinheim, Ger.) **4**, 416 (1992).
[7] D. Ariosa, V. N. Tsaneva, and Z. H. Barber, IEEE Trans. Appl. Supercond. **15**, 2993 (2005).
[8] Z. Mori, K. Sakai, H. Ota, and R. Aoki, J. Low Temp. Phys. **105**, 1283 (1996).
[9] R. D. Narhe, M. D. Khandkar, K. P. Adhi, A. V. Limaye, S. R. Sainkar, and S. B. Ogale, Phys. Rev. Lett. **86**, 1570 (2001).
[10] B. Hinnemann, H. Hinrichsen, and D. E. Wolf, Phys. Rev. Lett. **87**, 135701 (2001).
[11] Results taken from an extensive study of growing conditions for La-doped Bi-2201 films by Claudia Cancellieri *et al.* (unpublished).
[12] N.-B. Park, Y.-P. Park, and J.-H. Kim, Curr. Appl. Phys. **3**, 483 (2003).
[13] W. L. Yang, H. H. Wen, Y. M. Ni, J. W. Xiong, H. Chen, C. Dong, F. Wu, Y. L. Qin, and Z. X. Zhao, Physica C **308**, 294 (1998).
[14] S. Hendricks and E. Teller, J. Chem. Phys. **10**, 147 (1942).
[15] B. D. Cullity, *Elements of X-Ray Diffraction*, 2nd ed. (Addison-Wesley, Reading, MA, 1978).
[16] A. Gauzzi and D. Pavuna, Appl. Phys. Lett. **66**, 1836 (1995).